INL/RPT-24-78038
Revision 1

Irradiation Results of Commercial Neutron and Gamma Sensors at the Ohio State University Research Reactor

July 2024

Report

Kevin Tsai
Idaho National Laboratory

Idaho National Laboratory

INL is a U.S. Department of Energy National Laboratory
operated by Battelle Energy Alliance, LLC

INL/RPT-24-78038
Revision 1

Irradiation Results of Commercial Neutron and Gamma Sensors at the Ohio State University Research Reactor

Report

Kevin Tsai
Idaho National Laboratory

July 2024

Idaho National Laboratory
Measurement Science Department
Idaho Falls, Idaho 83415

http://www.inl.gov

Prepared for the
U.S. Department of Energy
Office of Nuclear Energy
Under DOE Idaho Operations Office
Contract DE-AC07-05ID14517

Page intentionally left blank

ABSTRACT

This report serves to present the evaluation results of commercial radiation detectors (SPNDs) with the potential to accomplish the data objectives—having sufficient gamma and fast-neutron sensitivity—at temperatures near 650°C. The detectors chosen for evaluation are gamma ion chambers from Exosens (previously known as Photonis) models CRGA11 and CRGE32 and tantalum-based self-powered neutron detectors (Ta-SPND) from Mirion.

The evaluation was performed in a series of heat irradiations from ambient to 850°C in the 9.5-inch dry tube furnace at the Ohio State University Research Reactor (OSURR). Ion chamber counting curves were measured to evaluate sensor operability at temperature. Detector sensitivity to reactor power and temperature were measured and presented in curve fit parameters. The curve fit equations were used to identify the suggested operational temperatures based on reactor power.

Overall, it was evaluated that the CRGA11 was not significantly affected by temperatures up to 650°C and is operable—with higher temperature-contributed signals—up to 700°C. The CRGE32 was more affected by the high temperatures compared to the CRGA11. As a result of increasing temperature, the leakage current was a dominating factor. While the detector can operate up to 600°C and 700°C with lowered high voltage, it is not recommended unless a suitably strong gamma flux field is present. Finally, Ta-SPND did not demonstrate good performance beyond 350°C due to the presence of an unknown phenomenon at changing temperatures. The study of the phenomenon is an active research topic outside the scope of this project.

Page intentionally left blank

CONTENTS

FIGURES

TABLES

ACRONYMS

ASI	Advanced Sensors and Instrumentation
LWR	Light Water Reactor
OSURR	Ohio State University Research Reactor
SPND	Self-Powered Neutron Detector

Page intentionally left blank

Irradiation Results of Commercial Neutron and Gamma Sensors at the Ohio State University Research Reactor

1. INTRODUCTION

The use of neutron and gamma detectors plays an important role in monitoring and controlling reactors. Strongly correlated with reactor power, the neutron and gamma distribution within the reactor core are continuously monitored through in-core and ex-core detectors to ensure safe and efficient operational margins are maintained. Supported by the Advanced Reactor Demonstration Program, many advanced reactor concepts and demonstration experiments are being developed. [1] Some of these reactor concepts include operating in the fast neutron energy region for better fuel cycle management as well as higher temperatures (650°C and above) for increased efficiency and heat process applications. [2] However, these changes from the traditional light water reactors (LWR) significantly limit the availability of neutron and gamma detectors, both in-core and near-vessel ex-core, that can monitor the reactor.

This project therefore aims to evaluate detectors with the potential to accomplish the data objectives of having sufficient gamma and fast-neutron sensitivity at temperatures near 650°C. The detectors chosen for evaluation are gamma ion chambers from Exosens (previously known as Photonis) models CRGA11 and CRGE32 and tantalum-based self-powered neutron detectors (Ta-SPND) from Mirion.

The CRGA11 has a vendor specified maximum operating temperature at 600°C. The CRGE32 is an untested non-uranium design based on the CFUE32 fission chamber which was rated for 600°C. In the special case of the Ta-SPND, though available commercially, will be undergoing its first testing in a heated irradiation.

Ion chambers are a versatile type of gas-filled detector that can measure different types of radiation depending on its construction and operation. The basic construction of an ion chamber includes a gas-filled chamber with two electrodes. The electrodes are placed at an appropriate voltage for charge collection following a radiation-ionization event in the gas chamber. The collection of the charges generates the electric signal, whether pulse or current. For gamma ion chambers, the current mode is used. However, even for detectors built to withstand high temperatures, preliminary testing should be performed to measure leakage current contribution as well as the operational voltage for ionization region.

Self-powered neutron detectors have many advantages as in-core detectors. Their construction is simple and robust, taking the form of a mineral-insulated, metal-sheathed cable with the lead wire attached to a neutron-sensitive wire called the emitter. Additionally, the emitter passively generates an electric current in the radiation field proportional to the field strength, which results in a simple readout system without the need for a high-voltage power supply. With the exclusion of a high-voltage power supply, there is less concern for leakage current. In application, however, a displacement current has been observed from temperature changes above 550°C. [3]

To evaluate each detector's performance, they are irradiated in a dry tube furnace at the Ohio State University Research Reactor (OSURR) alongside other sensors from the Advanced Sensor and Instrumentation (ASI) Program supported by the U.S. Department of Energy. [3] [4] This project aims to identify the effects of temperature as well as any potential failure modes. This will help inform advanced reactor designers on the potential applicability of these detectors or accommodations required to successfully deploy these detectors.

2. EXPERIMENT SETUP

Heated irradiations at OSURR are carried out in the 9.5-inch diameter dry tube with a cylindrical furnace as shown in Figure 1. The sensors were inserted into the furnace with the neutron or gamma-sensitive region positioned at the peak flux and temperature region (Figure 2 and Figure 3). Within

this position at 450kW reactor power, the total neutron flux is measured to be 1.1 x 10^{12} n/cm^2/s and gamma dose rate in Si is measured to be 4.4 x 10^6 rad-Si/hr. [5]

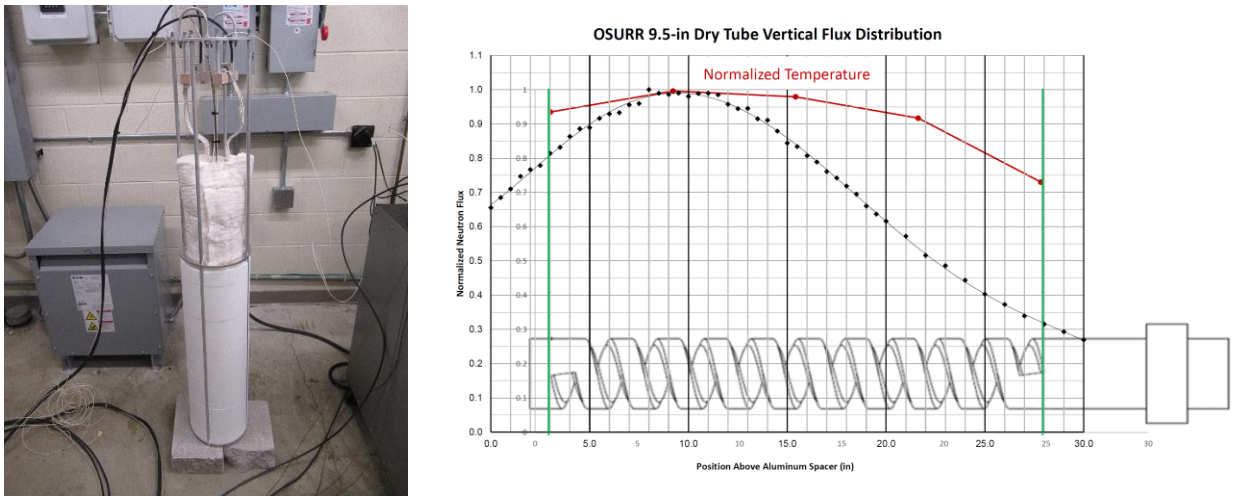

(a) (b)

Figure 1. (a) OSURR furnace rig. (b) Axial position of the furnace in relation to temperature and flux.

Sensor	[1]Probe tip height (in.)
CRGA11 x2	3
CRGE32	4.5
[2]HT FC x2	4.5
[2]Thermal FC	5
[2]Thx Rh-SPND	4.5
Type K #1	3
Type K #2	6
Type K #3	9

[1]referenced 0 per green line in Figure 1(b).
[2]Additional ASI sensors [4].

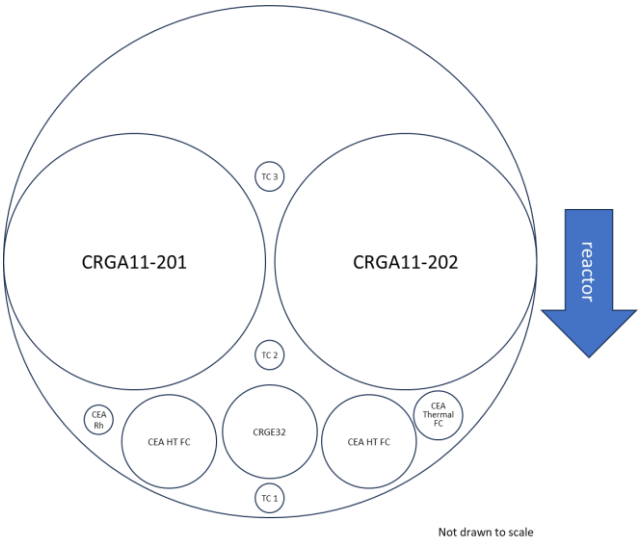

Figure 2. Sensor location in furnace rig for September.

Sensor	[1]Probe tip height (in.)
CRGA11 x2	3
CRGE32	4.5
Ta-SPND x2	0
[2]Rh-SPND-1	2.5
[2]Rh-SPND-2	6.5
Type K #1	6
Type K #2	3
Type K #3	3
Type K #4	20
[3]Type K #5, 6, 7	6

[1]referenced 0 per green line in Figure 1(b).
[2]Additional ASI sensors.
[3]OSU heater control.

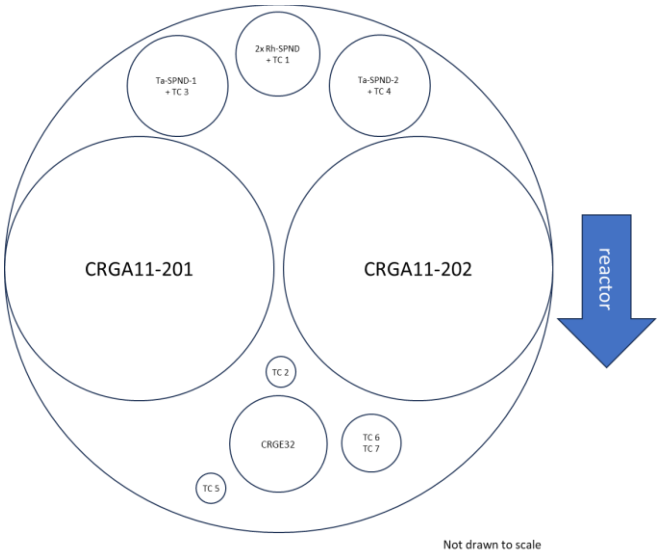

Figure 3. Sensor location in furnace rig for December.

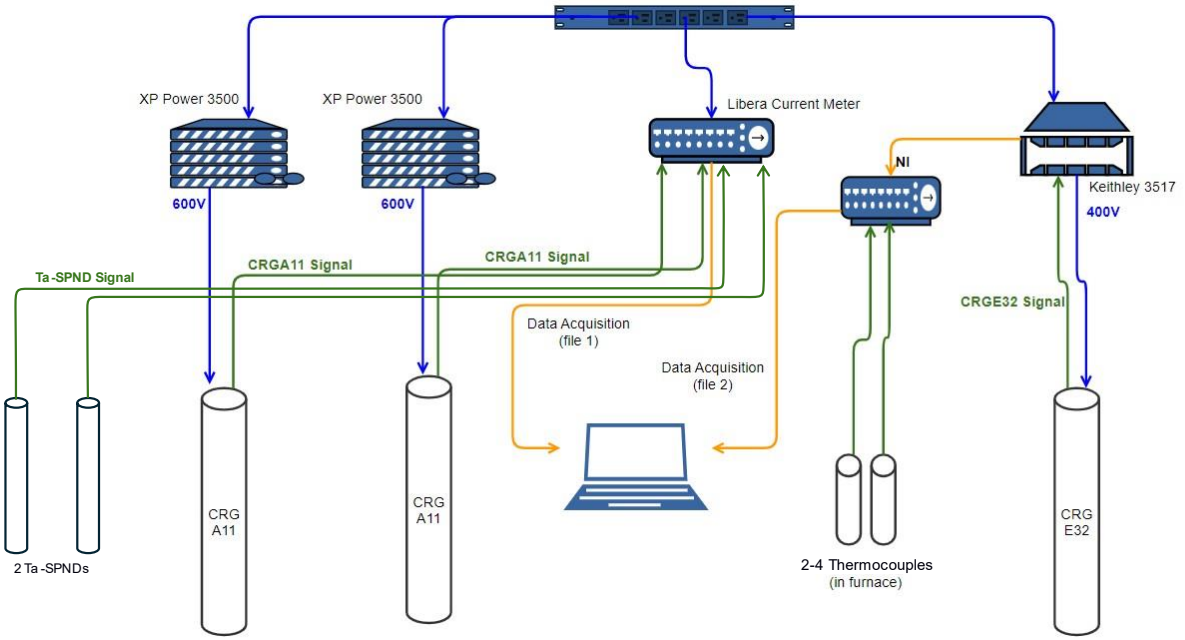

Figure 4. Schematic overview of detector electronics setup.

Two types of current meters were used for this experiment: Keithley 6517B for the CRGE32 and the Libera Current Meter for the two CRGA11s and the two Ta-SPNDs. The electronic setup is provided in Figure 4.

Since the CRGE32 uses a single coaxial cable for power and signal transmission, a Keithley 6517B was used in source voltage measure current (SVMI) mode to both provide the high voltage (set to 400V) and measure the detector current output. To log the data, the analog output of the from the Keithley 6517B that provided an inverted ±2V output per $\mp 2 \times 10$xA range was connected to a National Instrument (NI) acquisition system outfitted with NI with LabVIEW interface and recording data at the rate of 10 Hz.

Given the design of the CRGA11s with separated power and signal cables, the detector current output could be measured and recorded alongside the Ta-SPND current output using an Instrumentation

Technologies Libera Current Meter. The Libera Current Meter was set to measure in auto-range mode and record in slow data stream mode (10 Hz) with a graphical update rate of 10 seconds (100 data points) and automatic download at 1000 seconds (10,000 data points). Separately, two XP Power HCP-140-3500 were used to supply 600V to each of the CRGA11.

Several 1/16-inch type K thermocouples (TC) were used to provide temperature measurements for the sensors evaluation as well as controlling the heater. The TCs used for the sensors are integrated into the NI acquisition system via a TC reader card and data logged (10 Hz recording) alongside the CRGE32. The TCs used for the heater controller are connected directly to the controller system and are not available. For analysis purposes, temperature data from Type K #2 was used for the CRGE32 and CRGA11s for both September and December tests. The average between Type K #3 and #4 were used for the Ta-SPNDs for the December test. Timestamp matching between different acquisition systems (including the reactor ex-core data) are performed using data interpolation.

The overall project contained two series of irradiations performed in September and December. Experiments conducted in September included only the ion chambers at high power, 1 to 200kW reactor power. The December experiments were conducted at both low and high power, 10 to 30W and 1 to 100kW reactor power, respectively. Each experiment consisted of 3 days of irradiation over different power levels and temperatures. The irradiation plan for all irradiation is given in Table 1 and Table 2. It should be noted that the designated temperatures in the irradiation plan are used as temperature setpoints for the heater controller as measured by Type K #5, 6, and 7; therefore, the actual temperatures of each detector as measured by Type K # 2, 3, and 4 will vary.

Table 1. September irradiation plan for tests 1–3.

Test #1			Test #2			Test #3		
Power	Hold Duration	Temperature	Power	Hold Duration	Temperature	Power	Hold Duration	Temperature
100 W	1 hour	Ambient	100 W	1 hour	Ambient	100 W	15 min each	Ambient 600°C 650°C 700°C 750°C
1 kW 10 kW 100 kW 200 kW	15 min each	Ambient	1 kW 10 kW 100 kW 200 kW	15 min each	Ambient	1kW 10 kW 100kW 200kW 450kW	15 min each	750°C
1 kW	Raise temperature to 350°C		1 kW	Raise temperature to 650°C		1kW	Raise temperature to 850°C	
1 kW 10 kW 100 kW 200 kW	15 min each	350°C	1 kW 10 kW 100 kW 200 kW	15 min each	650°C	1kW 10kW 100kW	15 min each	850°C
1 kW	Raise temperature to 600°C		1 kW	Raise temperature to 700°C				
1 kW 10 kW 100 kW 200 kW	15 min each	600°C	1 kW 10 kW 100 kW 200 kW	15 min each	700°C			

Table 2. December irradiation plan for tests 1–3.

Test #1			Test #2			Test #3		
Power	Hold Duration	Temperature	Power	Hold Duration	Temperature	Power	Hold Duration	Temperature
10-30W	30 min each	Ambient 550°C 575°C 600°C 625°C 650°C 675°C 700°C	100 W	1 hour	Ambient	100 W	1 hour	Ambient
			1 kW 10 kW 100 kW	15 min each	Ambient	1 kW 10 kW 100 kW	15 min each	Ambient
			1 kW	Raise temperature 350°C		1 kW	Raise temperature 700°C	
			1 kW 10 kW 100 kW	15 min each	350°C	1 kW 10 kW 100 kW 200 kW	15 min each	700°C
			1 kW	Raise temperature 600°C		1 kW	Raise temperature 850°C	
			1 kW 10 kW 100 kW	15 min each	600°C	1 kW 10 kW 100 kW	15 min each	850°C
			1kW	30min each	625°C 650°C			

3. RESULTS

Overviews of both irradiation series are given in Figure 5 and Figure 6. The plots show detector responses to temperature and reactor power in a time-based plot. More detailed analysis on detector sensitivity and temperature effects are provided in the following subsections. In regard to the figures below, please note:

1. Figure 5(a)–Thermocouples tracking detector temperatures were swapped between TC-1 and TC-3.
2. Figure 5(c)–The high-voltage for the CRGE32 was turned off upon approaching 750°C near the 10.5-hour mark to prevent damage due to large leakage current. The detector was later returned to operation at a lower voltage (100V).
3. Figure 6(a)–Near the 14.75-hour mark, Ta-SPND-2 was removed from the current meter for a resistance measurement at temperature. However, the effect from the measurement did not recover until the next day.
4. Figure 6(a)–Near the 16-hour mark, counting curves were performed on both CRGA11 detectors.

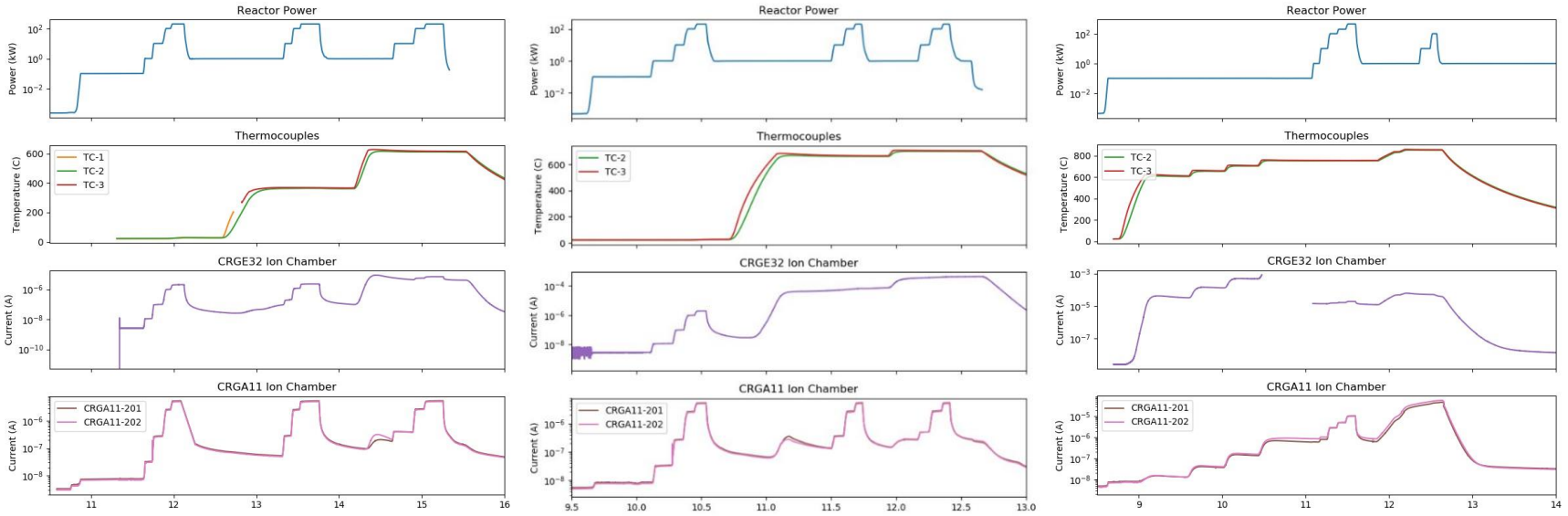

(a) (b) (c)

Figure 5. September irradiation overview for 1–200kW reactor power at (a) 600°C max temperature, (b) 700°C max temperature, and (c) 850°C max temperature.

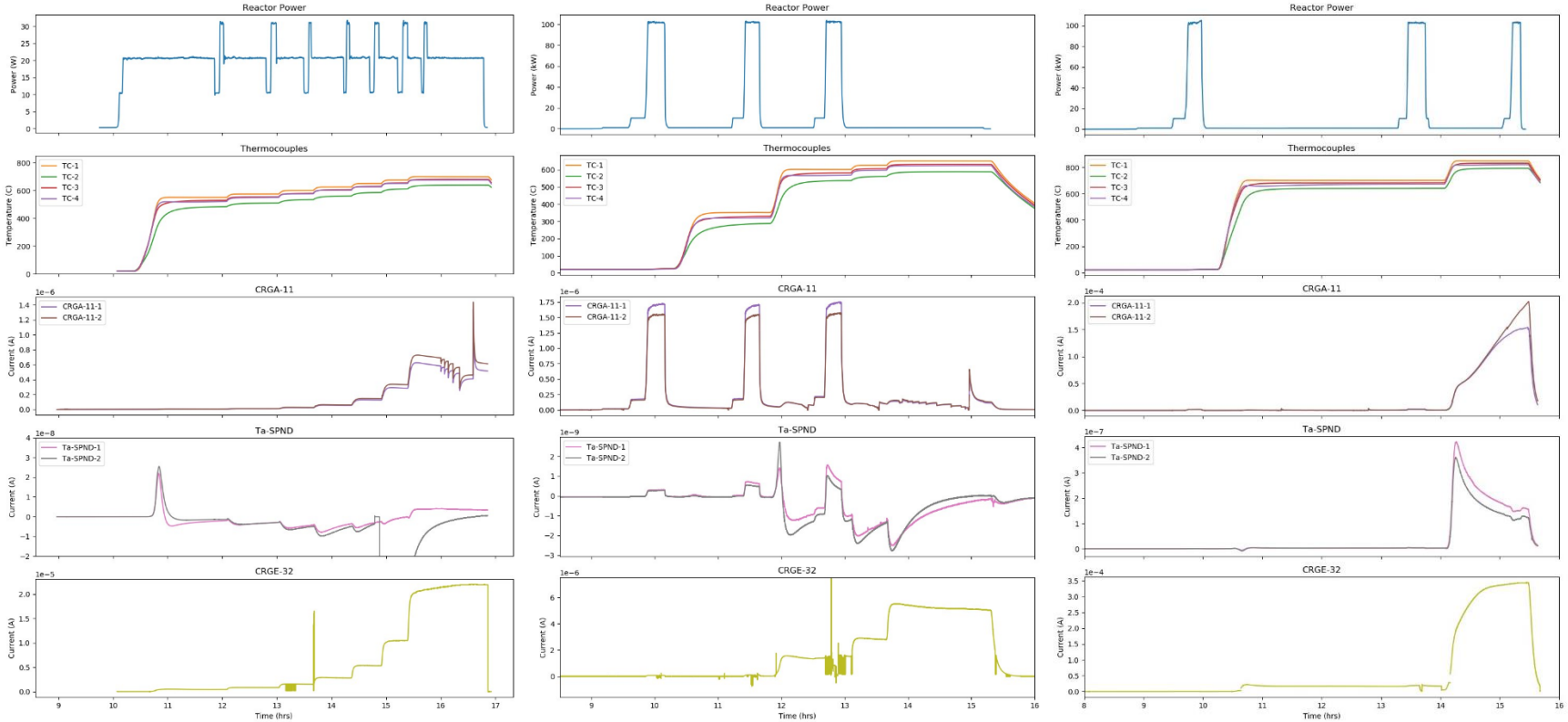

(a) (b) (c)

Figure 6. December irradiation overview for (a) 10–30W reactor power and 700°C max temperature, (b) 1–100kW reactor power and 650°C max temperature, and (c) 1–100kW reactor power and 850°C max temperature.

3.1 Ion Chamber Counting Curves

As the name suggests, ion chambers are gas-filled detectors that operate in the ionization operating region as shown Figure 7.Figure 7 In the ionization region, the response of the detector in a fixed radiation field does not change with voltage. The ionization region is specific to each detector and is identified by generating counting curves, a process of varying voltage and measuring response in a steady radiation field. A voltage, typically 1/3 into the ionization region, is chosen as the operational voltage.

In elevated temperature applications, however, leakage current and gas behavior can change the counting curve and operational voltage. The process therefore needs to be performed at multiple temperatures to ensure the proper voltages are applied to the detector for future use.

The operation voltages of the CRGA11 and CRGE32 are provided in Figure 8. The CRGA11 counting curves are performed at 1kW reactor power while the CRGE32 are during 100kW reactor power. This is to ensure that there is a sufficient signal output from the detector as a function of applied voltages. Voltages are varied from 0 to 600V for the CRGA11, and 0 to 400V for the CRGE32. A linear and log scale of the CRGE32 counting curve is presented to better understand its behavior at higher temperatures.

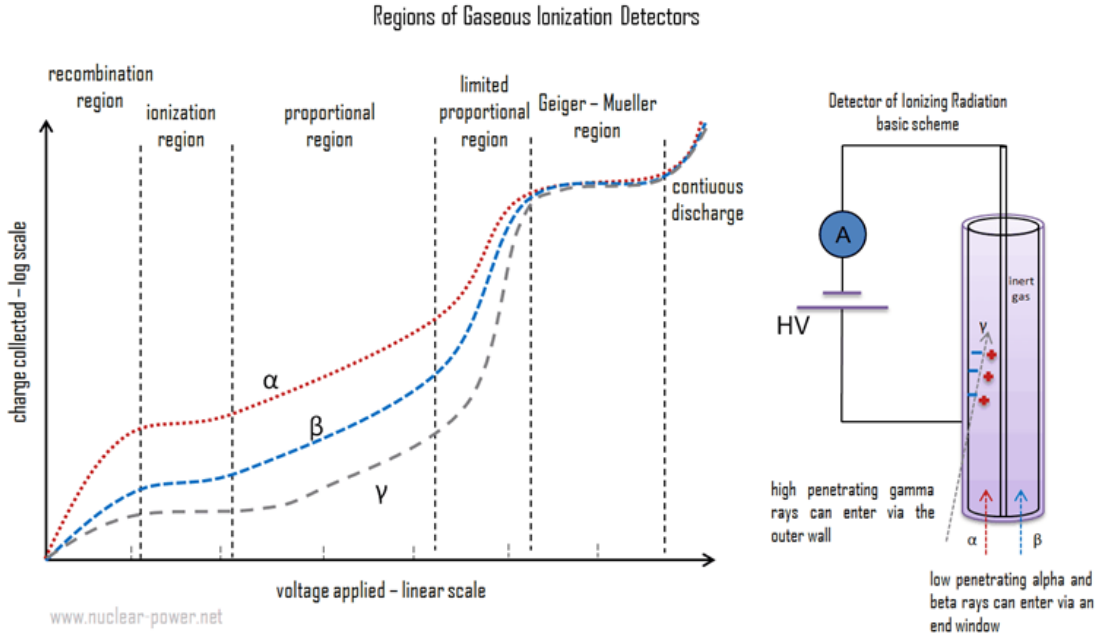

Figure 7. Operating regions of gas-filled detectors. [6]

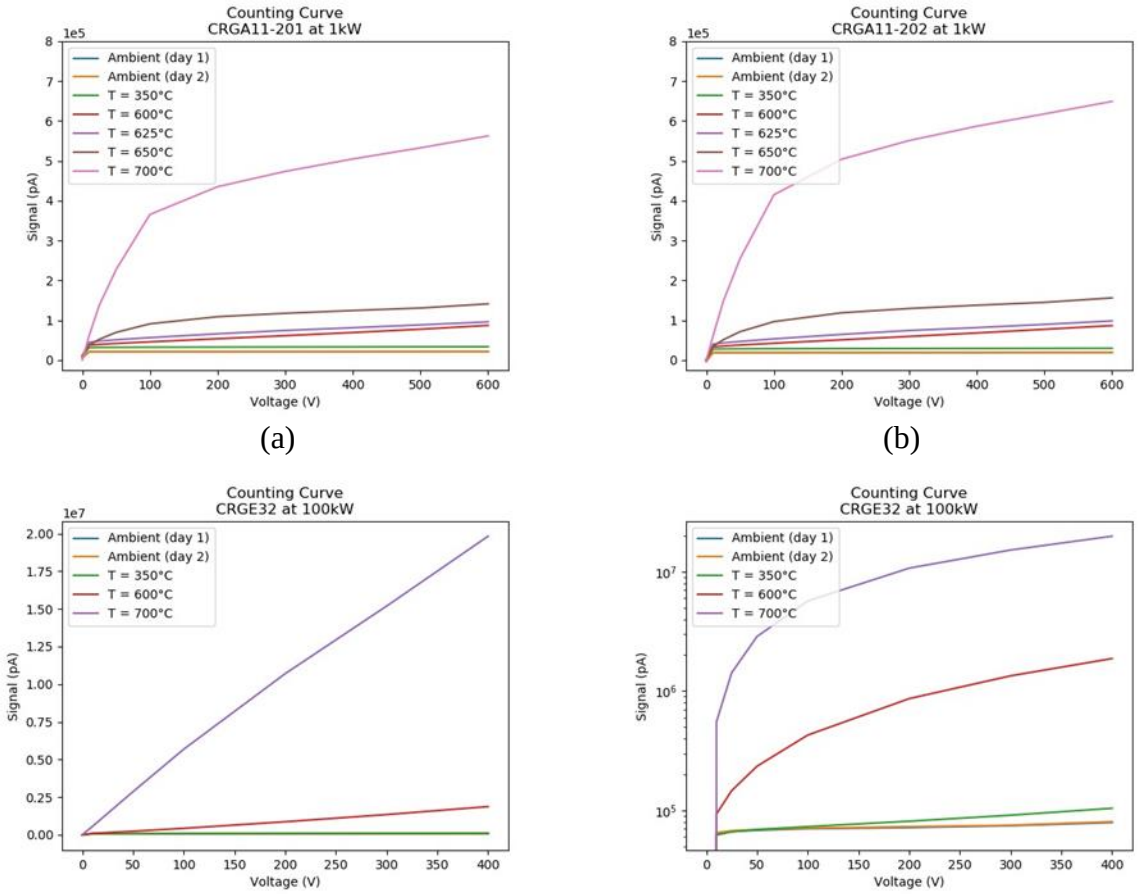

Figure 8. Counting Curves for (a) CRGA11-201, (b) CRGA11-202, (c) CRGE32 in linear-scale, and (d) CRGE32 in log-scale.

3.2 Detector Sensitivity

All three detectors operate in current mode with background current signal in the pico- to nanoamp range at zero power. Detector signals are measured from 0–100kW reactor power. As such, detector sensitivity curves–detector output per reactor power–are expressed in units of picoamps and kilowatts for different temperatures. The measured detector signal at different reactor power (P) at steady temperatures are all strongly linear, further shown by their r^2 value. As such, the linear curve fit parameters are defined as

$$Signal\ (pA) = a_1 + a_2 P \tag{1}$$

where a_1 represents the extrapolated zero-power background current is in picoamps, a_2 represents detector sensitivity in response to reactor power in picoamps/kilowatt. Fit parameters and further discussions on detector sensitivity for each detector type and model are provided in the following subsections.

3.2.1 CRGA11

Detector sensitivity to reactor power was measured from both September and December campaigns. A comparison of sensitivity curves for the two CRGA11s are shown in Figure 9 and the fit parameters are provided in Table 3. Additional sensitivity study for low-level detector sensitivity during reactor startups of the September tests are provided Figure 10 and Table 4.

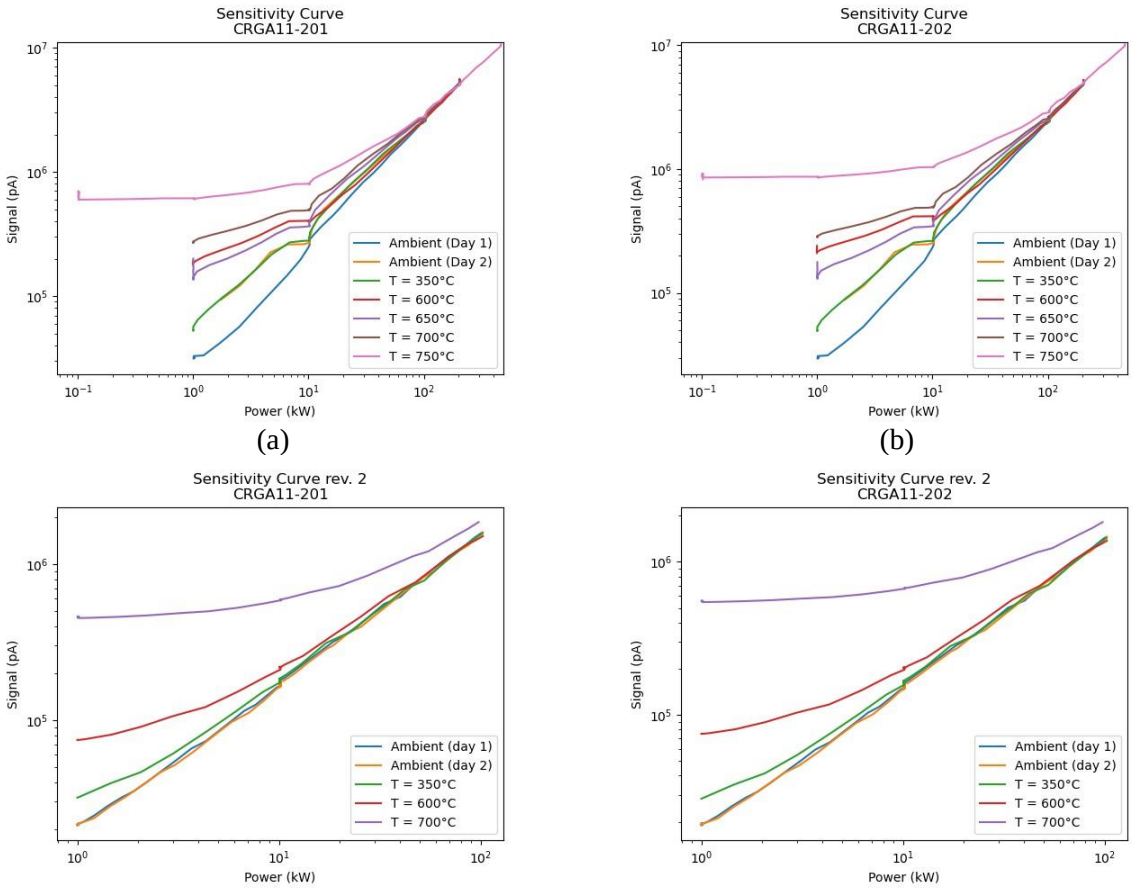

Figure 9. CRGA11 Overall sensitivity curve for (a) CRGA11-201, (b) CRGA11-202 in September tests; and (c) CRGA11-201, (d) CRGA11-202 in December tests.

Table 3. CRGA11 overall sensitivity curve fit parameters.

Sensor	Parameter	Ambient (day 1)	Ambient (day 2)	Temperature (°C)				
				350	600	650	700	750
CRGA11-201 (Sept.)	a_1	5.97E+03	5.53E+04	3.21E+04	1.37E+05	1.41E+05	2.73E+05	6.49E+05
	a_2	2.60E+04	2.53E+04	2.61E+04	2.59E+04	2.53E+04	2.46E+04	2.12E+04
	r^2	1.00E+00	9.99E-01	9.99E-01	9.99E-01	9.99E-01	9.99E-01	1.00E+00
CRGA11-202 (Sept.)	a_1	5.39E+03	5.21E+04	2.99E+04	1.55E+05	1.33E+05	2.86E+05	8.91E+05
	a_2	2.46E+04	2.39E+04	2.46E+04	2.43E+04	2.38E+04	2.31E+04	1.98E+04
	r^2	1.00E+00	9.99E-01	9.99E-01	9.99E-01	9.99E-01	9.99E-01	1.00E+00
CRGA11-201 (Dec.)	a_1	1.42E+04	1.56E+04	2.75E+04	7.05E+04	--	4.43E+05	--
	a_2	1.57E+04	1.53E+04	1.52E+04	1.46E+04	--	1.44E+04	--
	r^2	9.99E-01	1.00E+00	9.99E-01	9.98E-01	--	9.99E-01	--
CRGA11-202 (Dec.)	a_1	1.22E+04	1.32E+04	2.39E+04	6.97E+04	--	5.38E+05	--
	a_2	1.42E+04	1.39E+04	1.38E+04	1.31E+04	--	1.30E+04	--
	r^2	9.99E-01	1.00E+00	9.99E-01	9.99E-01	--	9.99E-01	--

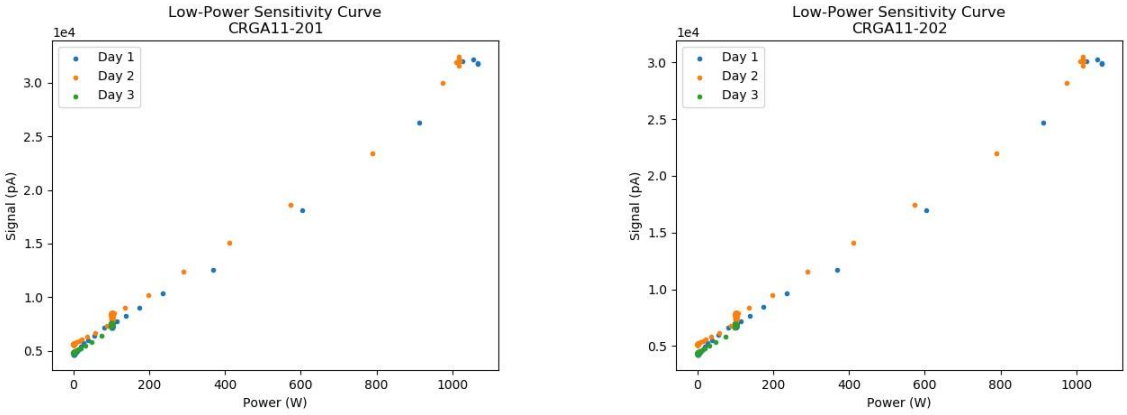

(a) (b)

Figure 10. CRGA11 low-power sensitivity curve for (a) CRGA11-201 and (b) CRGA11-202.

Table 4. CRGA11 low-power sensitivity curve fit parameters.

Sensor	Parameter	Day 1	Day 2	Day 3
CRGA11-201	a_1	4.91E+03	5.70E+03	4.82E+03
	a_2	2.50E+04	2.54E+04	2.63E+04
	r^2	9.95E-01	9.96E-01	9.97E-01
CRGA11-202	a_1	4.50E+03	5.22E+03	4.35E+03
	a_2	2.36E+04	2.40E+04	2.49E+04
	r^2	9.95E-01	9.96E-01	9.97E-01

Overall, the performance of both CRGA11s were very close to each other with an average sensitivity difference (% difference of parameter a_2) of 6.1% for the entirety of the September tests.

The fit parameters to detector sensitivity also provides further insight into detector behavior at temperature. As identified from a_1, the extrapolated zero-power background current output increased with increasing temperature. This is strongly suggestive of the increasing leakage current contribution from decreasing insulation resistance of the detector and cable (at a high operational voltage) at higher temperatures. The leakage current is generally observed as a direct current offset to all measurements at the same temperature. This is further substantiated by parameter a_2 remaining largely constant up to 650°C. This means that aside from a consistent leakage current, the detector behavior did not suffer sensitivity loss.

However, with irradiation progressing into 700 and 750°C, the decrease of parameter a_2 while remaining strongly linear (provided by $r^2 = 0.99$) suggests a drop in overall sensitivity. The causes for the sensitivity drop are presently unknown, but it is further observed in the December tests suggesting the mechanisms behind the sensitivity drop are nonrecoverable and potentially have a slow effect over time.

3.2.2 CRGE32

The CRGE32 was also tested in both September and December campaigns. The sensitivity curve and fit parameters are therefore provided in Figure 11 and Table 5. Additionally, detector noise had increased significantly in the December test, so a scatter plot was used for Figure 11(b).

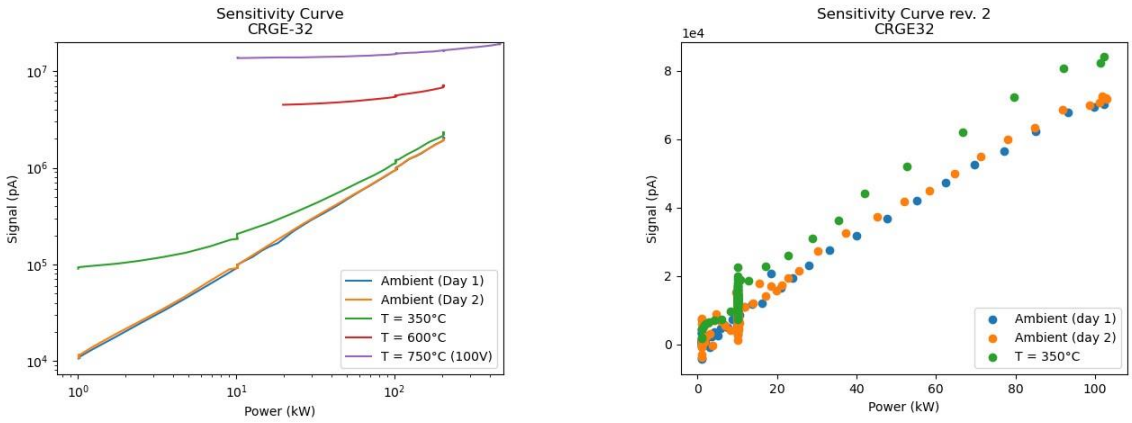

(a) (b)

Figure 11. CRGE32 overall sensitivity curve (a) during the September test and (b) during the December test.

Table 5. CRGE32 overall sensitivity curve fit parameters.

Sensor	Parameter	Ambient (day 1)	Ambient (day 2)	Temperature (°C)				
				350	600	650	700	750
CRGE32 (Sept.)	a_1	-4.38E+03	7.91E+02	8.10E+04	4.12E+06	--	--	1.40E+07*
	a_2	9.75E+03	9.54E+03	1.08E+04	1.43E+04	--	--	1.14E+04*
	r^2	9.99E-01	1.00E+00	9.99E-01	9.89E-01	--	--	9.92E-01
CRGE32 (Dec.)	a_1	7.56E+02	1.11E+03	5.50E+03	--	--	--	--
	a_2	7.21E+02	7.19E+02	8.12E+02	--	--	--	--
	r^2	9.73E-01	9.81E-01	9.71E-01	--	--	--	--
*CRGE32 operated at 100V								

Overall, the detector demonstrated satisfactory performance up to the expected rated temperature of 600°C and resolution necessary to operate at 750°C with a lowered voltage power supply during the initial testing in September. However, detector noise was observed as an issue especially in the December campaign. A large portion of the electrical noise contribution was suspected to be from the interconnect between the CRGE32 and the Keithley 6517B to operate in SVMI mode, but further investigation was unavailable during the campaign.

Similar to the CRGA11s, the CRGE32 also shows a reduction in sensitivity, provided by parameter a_2, between the September and December tests. This also suggests a non-recoverable degradation of the detector, but due to the observed electrical noise, direct comparison in sensitivity between the two campaigns is limited.

3.2.3 Ta-SPND

The Ta-SPNDs were only available for the December test campaign. The sensitivity curves are provided by Figure 12 and Table 6. Due to the low-sensitivity of the detector, the Libera Current meter was operated at the lowest range and showed a zero-power offset signal as a negative value as seen by parameter a_1. The negative value is considered as a current meter calibration offset and is not observed to have any further effect on detector behavior as presented by the ambient and 350°C data.

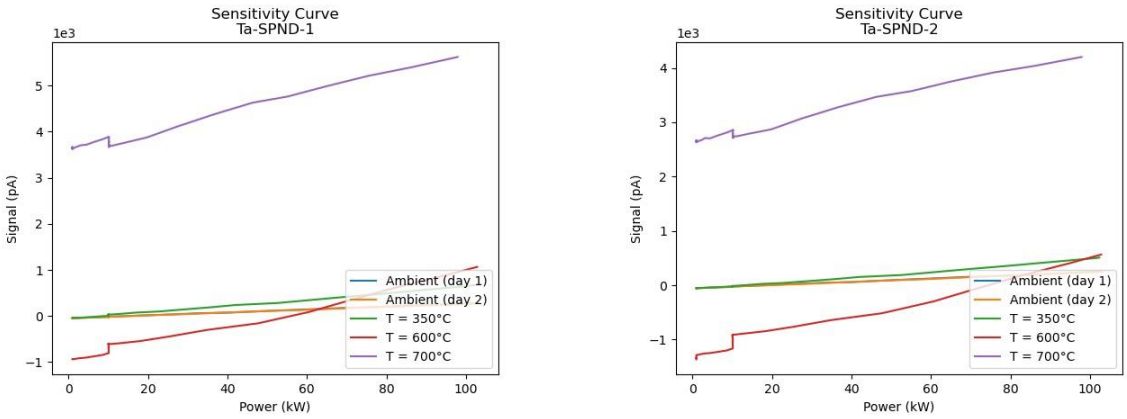

(a) (b)

Figure 12. Ta-SPND overall sensitivity curve for (a) Ta-SPND-1 and (b) Ta-SPND-2.

Table 6. Ta-SPND overall sensitivity curve fit parameters.

Sensor	Parameter	Ambient (day 1)	Ambient (day 2)	Temperature (°C)		
				350	600	700
Ta-SPND-1	a_1	-4.89E+01	-5.16E+01	-4.81E+01	-8.79E+02	3.60E+03
	a_2	3.19E+00	3.19E+00	6.89E+00	1.87E+01	2.02E+01
	r^2	9.99E-01	9.99E-01	9.96E-01	9.42E-01	9.59E-01
Ta-SPND-2	a_1	-5.58E+01	-5.79E+01	-6.42E+01	-1.21E+03	2.62E+03
	a_2	2.99E+00	2.98E+00	5.33E+00	1.75E+01	1.64E+01
	r^2	9.99E-01	9.99E-01	9.95E-01	9.04E-01	9.78E-01

Overall, the Ta-SPND operated well for its original intended application (ambient and 350°C). However, there is an observed sensitivity increase as a function of temperature. The sensitivity increase is most likely from the decrease in insulator resistance. Similar to the increasing leakage current observed in the ion chambers, a resistance drop in an SPND would allow electrons emitted from the emitter to have a higher probability to reach the collector-sheath and contributing to the detector output. In this case, this effect results in an increase in sensitivity instead of the DC offset.

Unexpectedly, a significant DC offset was observed at 600 and 700°C with opposite polarities. One potential cause for this effect is likely from the secondary detector output from radiation interactions in the insulator and sheath. For low temperature applications of SPNDs, the secondary detector output is significantly less than the emitter output; but with the lowered resistance at higher temperatures, the secondary outputs could become comparable to the emitter outputs.

3.3 Temperature Effects

As observed, all detectors have some sensitivity changes in response to temperature. This section serves to further describe the effects of temperature on detector response at 20W, 100W, and 1kW steady reactor power. This portion of the experiment is to provide better understanding of onset, dependence, and significance of temperature effects at different reactor power (i.e. to help calculate the significance of a 10% temperature contributed signal at 100W be for 1kW). The observed detector response to temperature (T) were empirically identified to have the functional form of

$$Signal(pA) = a_3 + a_4 T e^{a_5 T} \quad (2)$$

where a_3 is the extrapolated ambient steady-state signal, in picoamps, at the respective reactor power with a_4 and a_5 both being the temperature related parameters in units of pA/°C and °C^{-1}. Fit parameters for each detector as well as further discussions are presented in the following subsections.

3.3.1 CRGA11

Temperature effects in the CRGA11 were measured for both September and December campaigns. Temperature response curves and the fit parameters are provided in Figure 13, Figure 14, and Table 7. The 20W reactor power data is from the December tests. The 100W and 1kW reactor power data is from the September tests. The 20W and 100W data was a continuous data set while the 1kW data was only available as temperature hold points spread across multiple days. Additionally, the 20W data was further segmented to a 20–400°C range.

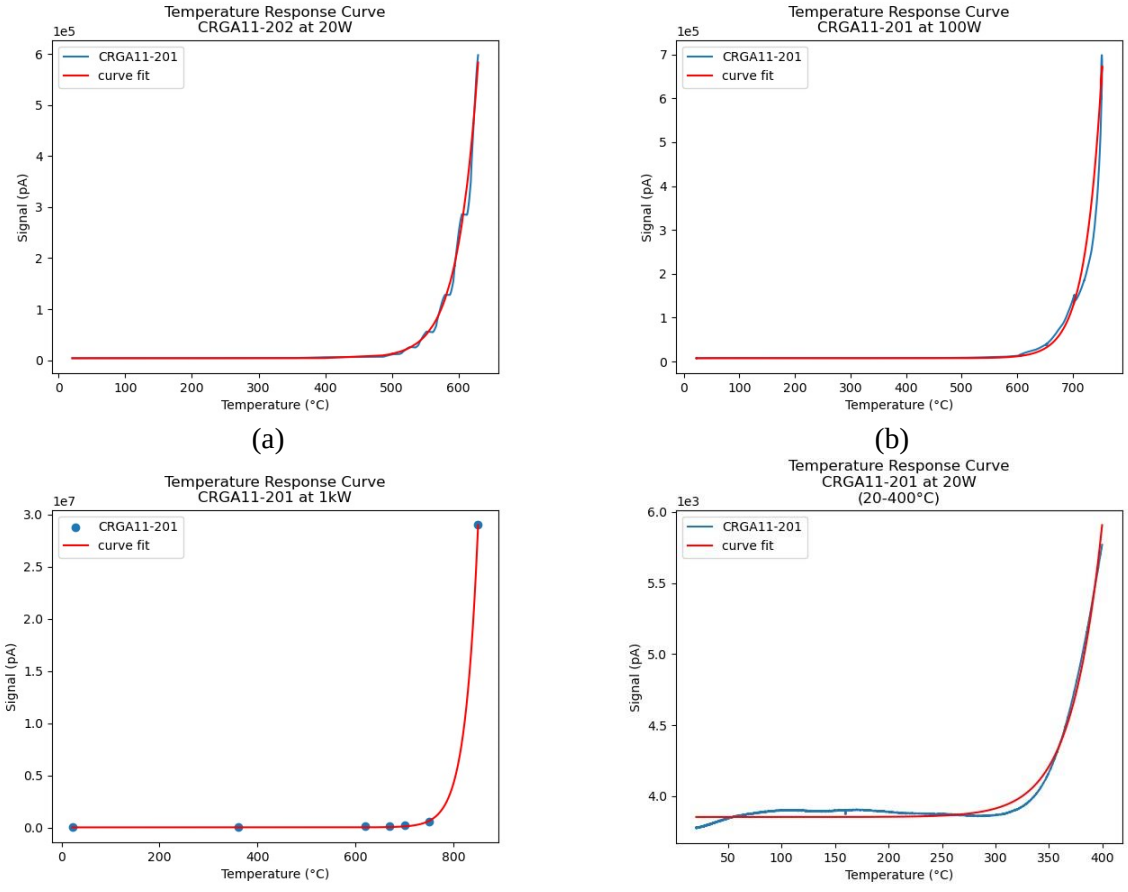

Figure 13. CRGA11-201 temperature response curve at (a) 20W, (b) 100W, (c) 1kW, and (d) 20W ambient to 400°C.

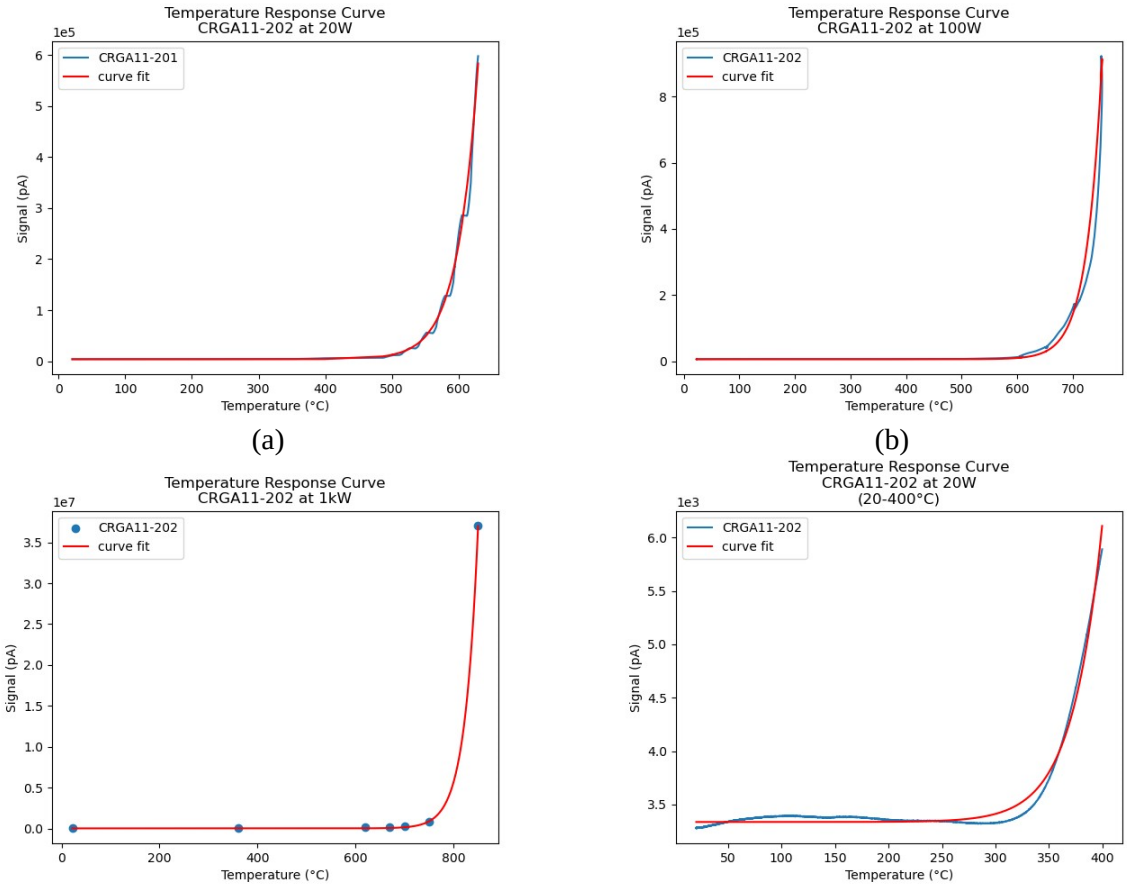

Figure 14. CRGA11-202 temperature response curve at (a) 20W, (b) 100W, (c) 1kW, and (d) 20W ambient to 400°C.

Table 7.CRGA11 temperature response curve fit parameters.

Sensor	Parameter	Reactor Power (W)			
		20	100	1000	20 (20–400°C)
CRGA11-201	a_3	3.79E+03	7.59E+03*	3.20E+04*	3.85E+03
	a_4	3.59E-06	4.28E-08	1.72E-09	1.13E-05
	a_5	3.08E-02	3.15E-02	3.63E-02	3.26E-02
CRGA11-202	a_3	3.65E+03	6.96E+03*	3.00E+04*	3.34E+03
	a_4	3.42E-06	6.18E-09	1.76E-09	1.17E-05
	a_5	3.11E-02	3.45E-02	3.63E-02	3.33E-02

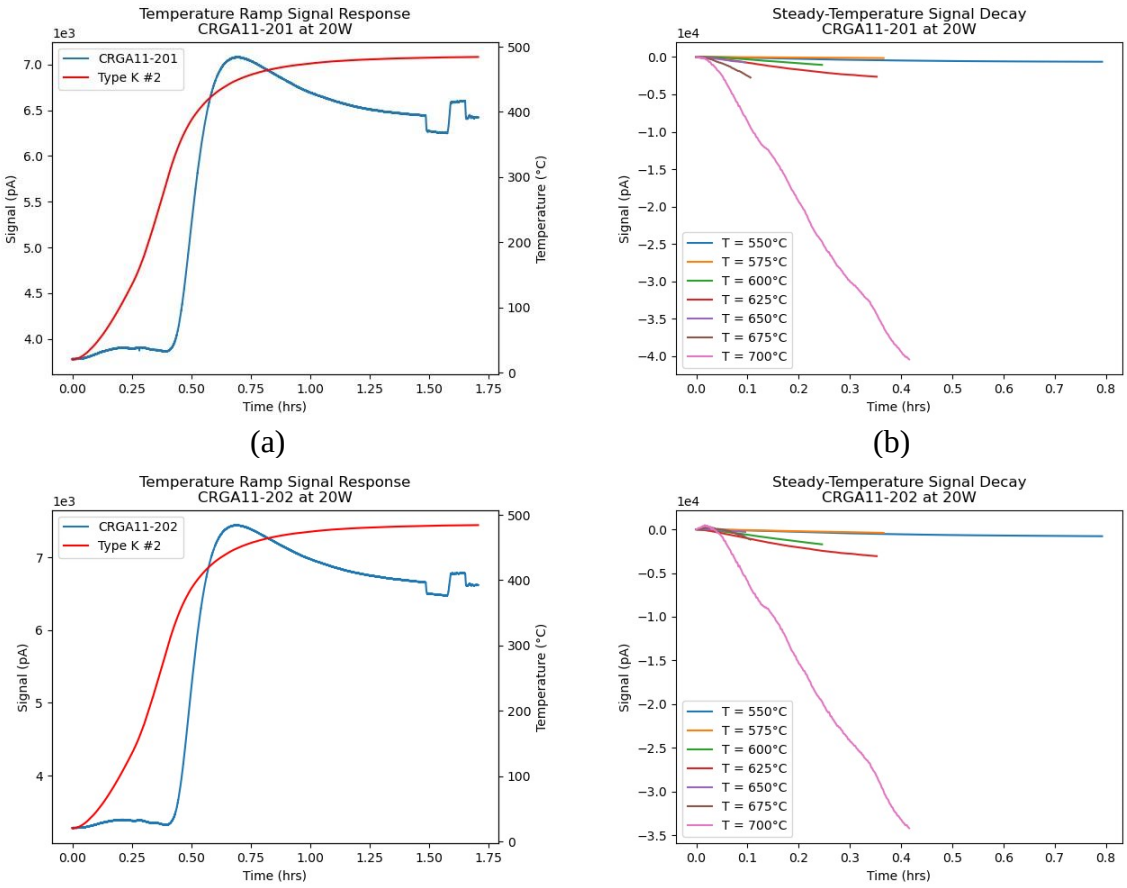

Figure 15. CRGA11 (a) and (c) An expanded view of the heat-and-hold at 500°C shows the maximum signal and subsequent decay prior to reactor power change. (b) Decay plots at steady temperature and power following a heat ramp. The values are subtracted from the peak signal—time and magnitude—for decay rate comparison.

During the campaign it was observed that the detector current following a heat ramp to steady temperature will overshoot with a maximum value occurring near the temperature hold points – either before or within a temperature variance threshold of less than 5°C. An example is presented in Figure 15(a) and (c) where the signal peaked before the threshold. Additionally, upon reaching a peak value, the signal will undergo a decay to a steady output with a very long time constant. The time constant also decreases with increasing temperature as shown in Figure 15(b) and (d) with zero time defined as reaching the 5°C variance threshold except for the first heat up to 500°C (35°C threshold) due to a long wait necessary for the furnace to stabilize. It should also be noted that the decay signals have a different functional form than a simple exponential decay function, thus it was not possible to extract an exact decay constant.

The signal overshoot is theorized to be electron discharges from the insulator as a function of temperature that is observed in SPNDs [3], [7]. However, the largest contributor of the temperature effects is still the final magnitudes of the steady-temperature signals up to 700°C. This steady-temperature signal is the leakage current contribution discussed in the prior section. The insignificance of the overshoot is also provided by the small magnitude of decay shown in Figure 15(b) and (d) relative to the overall signal change observed in Figure 13(a) and Figure 14(a).

3.3.2 CRGE32

The CRGE32 was also available for temperature analysis for both September and December campaigns. Detector signal change as a function of temperature at 20W, 100W, and 1kW steady-state reactor power are provided in Figure 16 and Table 8.

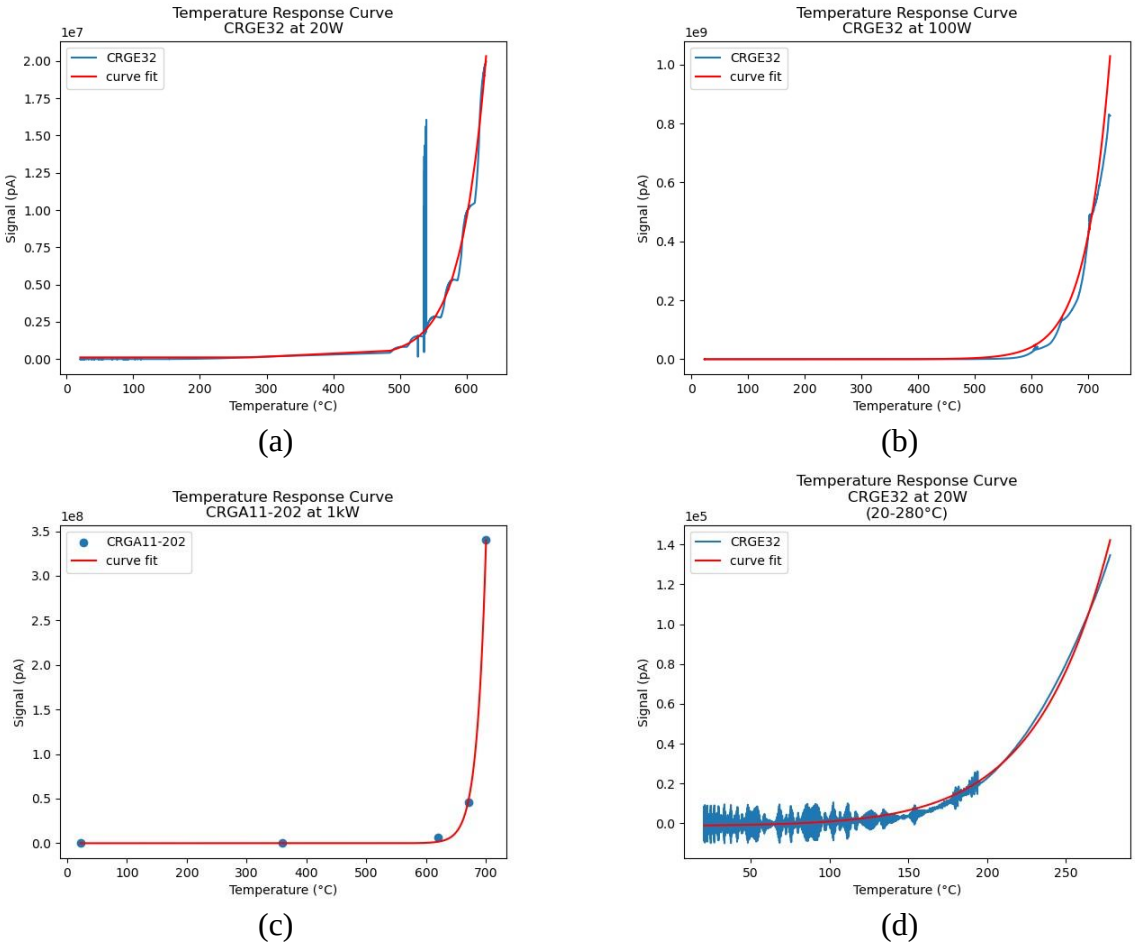

Figure 16. CRGE32 temperature response curve at (a) 20W, (b) 100W, (c) 1kW, and (d) 20W ambient to 280°C.

Table 8. CRGE32 temperature response curve fit parameters.

Sensor	Parameter	Reactor Power (W)			
		20	100	1000	20 (20—280°C)
CRGE32	a_3	1.13E+05	2.61E+03*	1.10E+04*	-1.16E+03
	a_4	5.98E-03	1.52E-01	9.04E-15	3.38E+00
	a_5	2.46E-02	2.17E-02	6.49E-02	1.81E-02

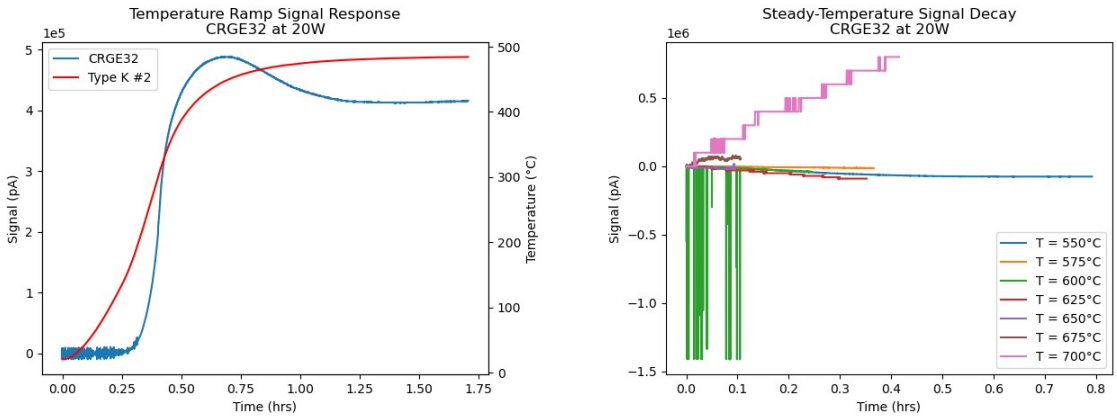

(a) (b)

Figure 17. CRGE32 (a) An expanded view of the heat-and-hold at 500°C to show the maximum signal. (b) Signal drift at steady temperature and power following a heat ramp. The values are subtracted from the peak signal—time and magnitude—for decay rate comparison.

Similar to the CRGA11s, the CRGE32 also shows a signal overshoot related to insulator discharge at each temperature hold for much of its operation (shown in Figure 17(a)). Exceptions to this behavior occur at 675°C where the signal continuously increased despite the temperature being head at 5°C variance (Figure 17(b). Nonetheless, the discharge current remains relatively insignificant when compared to the leakage current contribution.

However, coupling the unknown increasing current above the 675°C hold points as well as the increased detector noise for most of the December tests. It is assumed that the degradation suffered from the September test was more severe than the CRGA11 and that an unknown failure mode had appeared above 675°C.

3.3.3 Ta-SPND

The Ta-SPNDs were only available for testing for the December campaign. An overview of the temperature response of the Ta-SPNDs up to 700°C is shown in Figure 18. Since the Ta-SPND does not use a high voltage power supply, it is estimated that the stabilized increased current that is related to leakage current is zero. The remaining observed effect should therefore be the overshoots observed in the past experiments theorized to be electron discharge from the insulator as a function of temperature. However, the discharge pattern observed for the Ta-SPND in this campaign is significantly different from past experiments utilizing rhodium-based SPNDs [7]. Therefore, the applicable conclusion in proceeding forward is to consider the detector behavior for the initial heat up to 400°C (provided in Figure 19 and Table 9).

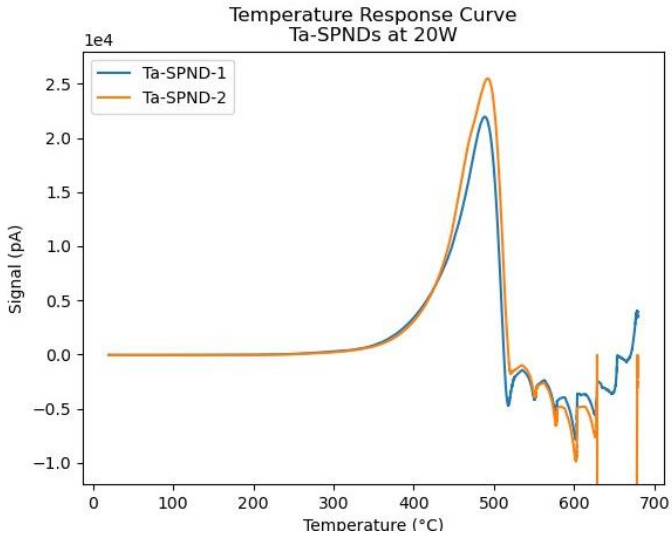

Figure 18. Ta-SPND temperature response curve at 20W steady power.

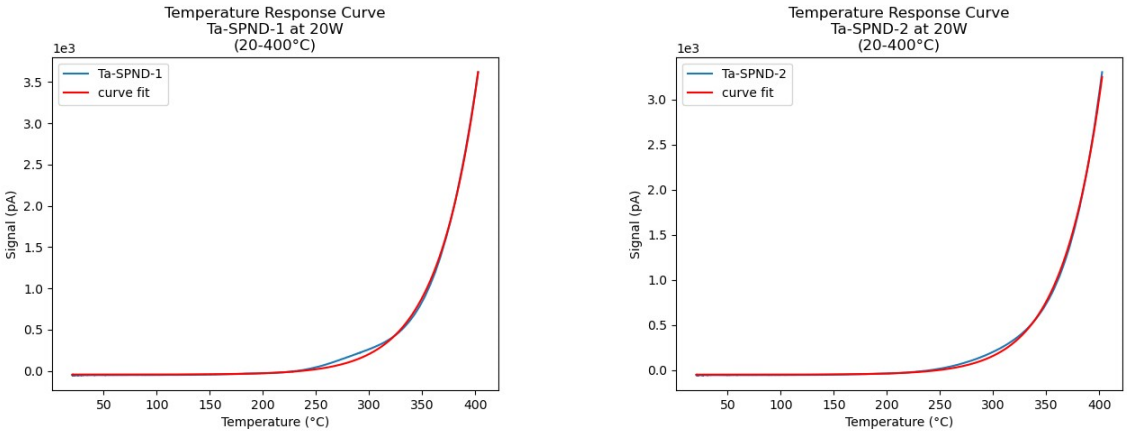

(a) (b)

Figure 19. Ta-SPND temperature response curve fit parameters for initial heat up.

Table 9. Ta-SPND temperature response curve fit parameters.

Sensor	Parameter	Reactor Power: 20W Temperature: 20 – 400°C
Ta-SPND-1	a_3	-4.33E+01
	a_4	7.52E-04
	a_5	2.34E-02
Ta-SPND-2	a_3	-5.16E+01
	a_4	5.12E-04
	a_5	2.41E-02

4. DISCUSSION

Based on the observed detector sensitivity and temperature-related effects, tables can be generated per detector type at desired operating power levels and suggested operating temperatures based on an arbitrary temperature-contributed signal or fluctuation. To demonstrate, a 10% threshold of temperature-contributed signal will be used.

$$Sensitivity \rightarrow Signal\ (pA) = a_1 + a_2 P \tag{3}$$

$$Temperature\ Effect \rightarrow Signal(pA) = a_3 + a_4 T e^{a_5 T} \tag{4}$$

To calculate the corresponding temperature based on power, the fit equations (with updated coefficient labeling) would need to be solved for *T* with some considerations:

1. While a_3 was a curve fit parameter, the value represents the signal at 20W and ambient temperature. Therefore, to use only the temperature-contributed signal, a_3 will be set to zero.
2. Averaged values of the sensitivity parameters at ambient will be used.

   In the case of the CRGA11, the September low-power parameter and December high-power parameters will be used where applicable to provide lower sensitivity for more conservative temperature calculation.
3. Ta-SPNDs will have parameter a_1 set to zero since the detector-electronic system had a negative signal measured outside of the reactor as well as in the experiment.
4. It should be noted that the CRGE32 and Ta-SPND have lower sensitivity. Therefore, the predicted temperatures ranges for low powers (<1kW) are near ambient temperatures.

With known parameters and desired power levels, the equations (3) and (4) can be used to solve for *T*:

$$T = W\left(\frac{0.1(a_1 + a_2 P)a_5}{a_4}\right)\left(\frac{1}{a_5}\right) \tag{5}$$

where W is the Lambert W function or product logarithm with all positive real values for all power and a 0.1 multiplier for the 10% threshold. Presented in Table 10 are the calculated values using the 10% threshold. This table shows the allowable temperature fluctuation from ambient at each power level.

Equation 5 is useful in providing a conservative estimation in application of these detectors, however, in actual practice, at steady temperatures at sufficiently long duration, the detectors have the potential to operate at a higher temperature. This is because of the high signal resolution.

With the temperature effects sufficiently settled, the temperature-related currents may be subtracted as a DC offset. For example, as shown in Figure 15(b)(d), even at 550°C, reactor power manipulations of 20W ± 10W were measurable. This is where a variation of Equation 5 may be used. By taking the derivative of Equation 4 with the same parameter considerations and solving for *T*, a temperature fluctuation limitation can be calculated (Equation 6). An application of this using the 10% threshold with 10°C allowable variation is presented in Table 11.

$$T = \left(W\left(\frac{0.1(a_1 + a_2 P)edT}{a_4}\right) - 1\right)\left(\frac{1}{a_5}\right) \tag{6}$$

Table 10. Estimated range of fluctuation between ambient and indicated temperature that has temperature-contributed signal less than 10%.

Sensor	Power (kW)	Est. Signal (pA)	[d]Temperature (°C)
CRGA11-201	0.01[a]	5.40E+03	361
	0.1[a]	7.70E+03	371
	1[a]	3.07E+04	411
	10[b]	1.70E+05	460
	100[b]	1.56E+06	524
CRGA11-202	0.01[a]	4.93E+03	351
	0.1[a]	7.11E+03	361
	1[a]	2.89E+04	400
	10[b]	1.53E+05	447
	100[b]	1.42E+06	510
CRGE32[c]	0.01	9.40E+02	19
	0.1	1.01E+03	20
	1	1.65E+03	28
	10	8.13E+03	69
	100	7.29E+04	148
Ta-SPND-1	0.01	3.19E-02	3
	0.1	3.19E-01	24
	1	3.19E+00	74
	10	3.19E+01	144
	100	3.19E+02	224
Ta-SPND-2	0.01	2.99E-02	5
	0.1	2.99E-01	28
	1	2.99E+00	81
	10	2.99E+01	151
	100	2.99E+02	229

[a] Based on September low-power data in Table 4.

[b] Based on December ambient data in Table 3.

[c] Based on December ambient data in Table 5.

[d] a_4 and a_5 data are all based on the 20W (20–400/500°C) parameter.

Table 11. Estimated highest temperature with ±10°C that has temperature-contributed signal less than 10%.

Sensor	Power (kW)	Est. Signal (pA)	[d]Temperature (°C) ± 10°C
CRGA11-201	0.01[a]	5.40E+03	524
	0.1[a]	7.70E+03	534
	1[a]	3.07E+04	574
	10[b]	1.70E+05	624
	100[b]	1.56E+06	690
CRGA11-202	0.01[a]	4.93E+03	509
	0.1[a]	7.11E+03	520
	1[a]	2.89E+04	560
	10[b]	1.53E+05	607
	100[b]	1.42E+06	671
CRGE32[c]	0.01	9.40E+02	221
	0.1	1.01E+03	224
	1	1.65E+03	248
	10	8.13E+03	323
	100	7.29E+04	431
Ta-SPND-1	0.01	3.19E-02	106
	0.1	3.19E-01	186
	1	3.19E+00	271
	10	3.19E+01	359
	100	3.19E+02	449
Ta-SPND-2	0.01	2.99E-02	113
	0.1	2.99E-01	192
	1	2.99E+00	275
	10	2.99E+01	361
	100	2.99E+02	448

[a] Based on September low-power data in Table 4.

[b] Based on December ambient data in Table 3.

[c] Based on December ambient data in Table 5.

[d] a_4 and a_5 data are all based on the 20W (20–400/500°C) parameter.

5. CONCLUSION

The purpose of this project is to evaluate three different sensors—CRGA11, CRGE32, and Ta-SPND—for high-temperature applications. Counting curves were performed on the CRGA11 and CRGE32. Detector sensitivity as a function of reactor power and temperature effects were measured. Using detector sensitivity and temperature response behaviors, an estimation of applicable temperature ranges was presented based on different power levels.

The counting curves suggest that the CRGA11 was not significantly affected by temperature up to 650°C and operable—with higher temperature-contributed signals—up to 700°C. The CRGA11 also has

the highest sensitivity. The results show that at a sufficiently high gamma flux field, the detector can operate even beyond its rated operational temperature of 600°C. However, in low gamma flux fields, it is suggested to lower the environmental temperatures.

The CRGE32 was more affected by the high temperatures compared to the CRGA11, as evident in the counting curve. The nearly linear behavior observed shows that the leakage current was a dominating factor. While the detector can operate up to 600–700°C with lowered high voltage, it is not recommended unless a suitably strong gamma flux field is present.

The Ta-SPND did not demonstrate good performance beyond 350°C. This is due to the coupled effects of low sensitivity and the presence of an unknown phenomenon at changing temperatures. The phenomenon is an active research topic outside the scope of this project.

6. REFERENCES

[1] DOE Nuclear Energy. 2020. "INFOGRAPHIC: Advanced Reactor Development." Accessed 30 November 2023, Department of Energy Office of Nuclear Energy. https://www.energy.gov/ne/articles/infographic-advanced-reactor-development.

[2] U.S. DOE. 2015. "Quadrennial Technology Review 2015 High Temperature Reactors Chapter 4: Technology Assessments." Accessed 30 November 2023, U.S. Department of Energy. https://www.energy.gov/sites/default/files/2016/03/f30/QTR2015-4J-High-Temperature-Reactors.pdf.

[3] Tsai, K., Reichenberger, M., and Palmer, J. 2021. "Comparative Assessment of Neutron Flux sensor Technologies for Advanced Reactors." INL/EXT-21-65635, Idaho National Laboratory. https://inldigitallibrary.inl.gov/sites/sti/sti/Sort_56134.pdf.

[4] Tsai, K., Reichenberger, M., de Izarra, G., and Barbot, L. 2024. "Performance Benchmark of Commercial and Developmental Fission Chambers in Elevated Temperatures." INL/RPT-23-75886, Idaho National Laboratory. https://inldigitallibrary.inl.gov/sites/sti/sti/Sort_80511.pdf

[5] OSU College of Engineering. n.d. "NRL Irradiation Facility Neutron Fluxes and Neutron & Gamma Dose Rates." Ohio State University, College of Engineering. https://reactor.osu.edu/facilities/research-reactor/nrl-irradiation-facility-neutron-fluxes-and-neutron-gamma-dose-rates.

[6] Nuclear Power. n.d. "Operating Regions of Ionizing Detectors – Detector Voltage." Accessed April 2024, Nuclear Power. https://www.nuclear-power.com/nuclear-engineering/radiation-detection/gaseous-ionization-detector/operating-regions-of-ionizing-detectors-detector-voltage/.

[7] Tsai, K. 2022. "Development of Temperature Compensation Tools for SPNDs Operating in High Temperature Environments." INL/RPT-22-69883, Idaho National Laboratory. https://inldigitallibrary.inl.gov/sites/sti/sti/Sort_64124.pdf.